SAND2024-01443J

Comparison of atmospheric radionuclide dispersion models for a risk-informed consequence-driven advanced reactor licensing framework

Jeffrey Wang[1], Daniel Clayton[2], Shaheen Azim Dewji[3,*]

[1]Nuclear and Radiological Engineering and Medical Physics Programs, Georgia Institute of Technology, Atlanta, GA, jeffreywang@gatech.edu

[2]Sandia National Laboratories, Albuquerque, NM, djclayt@sandia.gov

[3,*]Nuclear and Radiological Engineering and Medical Physics Programs, Georgia Institute of Technology, Atlanta, GA, shaheen.dewji@gatech.edu

*Corresponding author

0. Abstract

Current nuclear facility emergency planning zones (EPZs) are based on outdated distance-based criteria, predating comprehensive dose and risk-informed frameworks. Recent advancements in simulation tools have permitted the development of site-specific, dose, and risk-based consequence-driven assessment frameworks. This study investigated the computation of advanced reactor (AR) EPZs using two atmospheric dispersion models: a straight-line Gaussian plume model (GPM) and a semi-Lagrangian Particle in Cell (PIC). Two case studies were conducted: (1) benchmarking the NRC SOARCA study for the Peach Bottom Nuclear Generating Station and (2) analyzing an advanced INL Heat Pipe Design A microreactor's end-of-cycle inventory. The dose criteria for both cases were 10 mSv at mean weather conditions and 50 mSv at 95th percentile weather conditions at 96 h post-release. Results demonstrated that GPM and PIC estimated similar mean peak dose levels for large boiling water reactors in the farfield case, placing EPZ limits beyond current regulations. For ARs with source terms remaining in the nearfield, PIC modeling without specific nearfield considerations could result in excessively high doses and inaccurate EPZ designations. PIC dispersion demonstrated an order of magnitude higher estimate of nearfield inhalation dose contribution when compared to GPM results. Both models significantly reduced EPZ sizing within the nearfield. Thus, reductions in the AR source term may eliminate the need for a separate EPZ.

1. Introduction

Nuclear facilities, including power plants, have provided a safe, low-carbon, and economical source of baseload electricity. Nuclear energy's safety record is excellent, with exceedingly rare incidents resulting in radiological release. Therefore, public health and safety assurances remain paramount, addressed through safety and emergency planning. Globally, dozens of advanced reactor (AR) projects are underway, such as alternative coolant or small modular reactors (SMRs) for regional and international markets. These projects must undergo regulatory review and approval before construction can begin (Ramana et al., 2013). The primary concern is that existing regulatory guidance is tailored to large light water reactors (LWRs), and licensing AR designs under these requirements has faced significant delays and costly exceptions. One element of a safety plan that a nuclear power plant must implement,

according to regulations established by the US Nuclear Regulatory Commission (NRC), is a circular Emergency Planning Zone (EPZ) within the surrounding region (Moe, 2014).

The NRC recognizes in SECY-15-0077 that licensing a fleet of Ars under existing regulatory processes is an unnecessary burden upon the regulator and licensee and will require a tailored assessment of safety considerations specific to each system (Maioli, 2009; INL, 2010; Satorius, 2015). As such, siting considerations have been revisited in SECY-20-0045 for new next-generation fleets of advanced nuclear reactor designs, such as small modular (SMRs) and microreactors, which account for their design safety improvements and societal risk (Doane, 2022). Specifically, the next generation of ARs - notably SMRs and microreactors - have opted for smaller facility footprints and overall generation capacity for lower upfront capital costs and faster construction speed, improving their competitiveness against other energy sources. As part of the new regulatory framework for ARs, a comprehensive methodology should be employed that considers the potential hazards associated with the reactor and accordingly scales their EPZ. This approach should also address AR designs' integrated safety performance, implementing a performance-based, risk-informed, consequence-driven licensing process for new reactors.

Current NRC regulations define EPZ boundaries at 10 miles (16.6 km) for plume exposure pathways and 50 miles (80.5 km) for ingestion, regardless of simulated consequence models for most reactor designs in 10 CFR 50.47 (U.S. NRC, 2013). However, these radii were designed for large, pressurized water reactors (PWRs) with much larger radionuclide release quantities than ARs, notably microreactors. In SECY-11-0152, the NRC has discussed implementing a risk-informed scalable EPZ to address the reduced risk posed by ARs' smaller size and projected release inventory (Wiggins and Johnson, 2011). Active NRC rulemaking surrounding 10 CFR 50.160 and 10 CFR 53.855 has presented a modified risk-informed technical basis for delineating an EPZ that optimizes siting and licensing requirements for ARs, accounting for their inherent safety and reduced source terms (U.S. NRC, 2021; U.S. NRC, 2023). To address the NRC's proposed EPZ methodology, a new approach could increase reactor safety and promote NRC's efforts to credit AR safety features (U. S. Nuclear Regulatory Commission, 2020; Carless et al., 2019).

This new approach is already found to be in use internationally in accordance with IAEA safety standards and recommendations. Particularly, their suggested distribution of emergency planning zones is divided into a series of concentric regions of interest known as the Precautionary Action Zone (PAZ), Urgent Protective Action Planning Zones (UPZ), Extended Planning Distance (EPD), and Ingestion and Commodities Planning Distance (ICPD) (IAEA, 2013). The PAZ consists of an area closest to the facility boundaries where releases regardless of weather conditions and stochastic factors pose significant health risks to individuals. UPZ extends beyond the PAZ and is akin to the NRC's EPZ with a requirement for operators and local governments to proactively prepare inhabitants with preventive mitigation measures. EPD and ICPD encompass a large geographical region that focuses on long term monitoring and identification of hotspot concentrations that could pose a chronic danger. IAEA does not prescribe distances for each zone but rather dosimetric criteria of 1 Gy for the PAZ and 100 mSv (10 rem) for the UPZ. This can be compared to the proposed NRC dose threshold requirement of 50 mSv (5 rem) for the EPZ. Additionally, they specifically note that reactors less than 100 MWth are unlikely to generate exposure levels that necessitate offsite emergency planning and hence recommended that no emergency zones are required for operation. This conclusion will be corroborated in this paper with the results of the mean peak doses from the 5 MWth High Temperature Gas Cooled Reactor release scenario.

Atmospheric transport analysis of aerosolized radionuclide source terms, typically generated for all historical weather conditions at the facility, is crucial in estimating the potential consequences of radioactive material dispersion and deposition into the environment. The two most common and NRC-recommended atmospheric transport and dispersion (ATD) models are the conventional Gaussian plume model (GPM) (also referred to in NRC regulatory guide 1.111 as Gaussian puff advection) and the Lagrangian particle in cell (PIC) model (U.S. NRC, 1977). The MELCOR Accident Consequence Code System (Maccs) code, developed by Sandia National Laboratories, implements both modeling pathways in a single interface, with its built-in GPM in conjunction with National Oceanic and Atmospheric Administration (NOAA) Hybrid Single-Particle Lagrangian Integrated Trajectory (HYSPLIT) PIC trajectory model (Leute et al., 2021).

Therefore, this study compared traditional GPM and PIC ATD models to develop a risk-informed consequence-driven designation of AR siting boundary estimates. The resulting EPZ boundary was designated based on the calculated peak dose distribution and appropriate risk assessment methodology. In this study, the use of advanced atmospheric transport modeling in the Maccs code interface with its built-in Gaussian model and HYSPLIT Lagrangian integration demonstrated a novel framework for calculating dose-based siting boundaries while evaluating the potential for scalability of EPZs for AR regulatory frameworks.

2. Methodology

The source term and radionuclide release timeline for the boiling water reactor (BWR) facility at the Peach Bottom Nuclear Power Plant were used as a benchmark of the NRC's State-of-the-Art Reactor Consequence Analysis (SOARCA) study (Bixler et al., 2013). A heat pipe-cooled microreactor concept was additionally selected as a representative AR due to its high potential for near-term deployment and low source term inventory. These cases were selected to investigate any improvements to EPZ siting evidenced by the proposed methodology (Wang et al., 2023). Risk is quantified using a total effective dose equivalent (TEDE) calculated using the ICRP Publication 60 methodology and weighting factor with stratified random sampled weather conditions from 2021. Harnessing state-of-the-art capabilities in Maccs provided the two ATD models (GPM and PIC) to disperse source terms in accordance with NRC Regulatory Guide 1.111 (U.S. NRC, 1977).

2.1. Gaussian Straight-Line Plume Mode (GPM)

The GPM dispersion model in Maccs assumes a Gaussian normal distribution of radionuclides in the crosswind plane and a straight-line outward trajectory with constant initial velocity and direction from the initial point. The plume is modeled with a Gaussian normal distribution in the vertical direction, centered on the release height and extending to the simulation boundaries, reflecting off the ground and upper atmospheric mixing layer. The model assumes negligible bulk settling velocity compared to atmospheric mixing. The plume concentration is considered uniform vertically after enough reflections (Nosek and Bixler, 2021). The general formula for concentration within a Gaussian plume is given by equation (1) (Clayton et al., 2022).

$$C(x,y,z) = \frac{Q}{2\pi\sigma_y\sigma_z\bar{u}} \cdot exp\left(\frac{-y^2}{2\sigma_y^2}\right)\left[exp\left(\frac{-(z-H)^2}{2\sigma_z^2}\right) + exp\left(\frac{-(z+H)^2}{2\sigma_z^2}\right)\right] \#(1)$$

where C is the concentration of the particulate generated by a source with strength Q at downwind (x), crosswind (y), and above ground (z) locations; H is the effective height of the plume centerline; and σ is the standard deviation of wind diffusion in the corresponding plane. Downwind, lateral, and vertical diffusion standard deviation values at different classes of atmospheric stability have been tabulated in NRC Regulatory Guide 1.145 (U.S. NRC, 1979).

The Maccs GPM dispersion model assumes a straight-line trajectory for each plume segment, regardless of changes in wind direction at the source. This model assumes even topography and weather conditions but addresses some concerns by discretizing source terms into hourly segments (Nosek and Bixler, 2021). This allows the model to capture some of the variability in wind direction beyond the initial release but does not fully account for the complex effects of atmospheric turbulence and other factors that can affect plume dispersion. For example, the model does not consider the effects of downwind buildings, mountains, or other obstacles. The model also assumes that the plume is evenly distributed within each Gaussian segment. This assumption is not always accurate, as the plume can become more concentrated in certain areas due to atmospheric turbulence and other factors. Despite these limitations, the Maccs GPM dispersion model is a widely used tool for estimating the dispersion of atmospheric pollutants. It is relatively simple to use and provides reasonable results for various applications.

2.2. Lagrangian Particle in Cell Model (PIC)

HYSPLIT simulates airborne particle dispersion using a PIC model that combines Eulerian and Lagrangian computational fluid dynamics approaches with the ultimate concentrations estimated from the simulated particle concentrations. Meteorological data at set temporal intervals is required to regularly repopulate the backing rectangular grid of necessary parameters in which a set of Lagrangian particles are advected and diffused. The combined three-dimensional velocity vectors are applied to the simulated particles using the following process implemented in HYSPLIT (Draxler and Hess, 1998). An initial guess position is found using the following equation (2) (Draxler and Hess, 1998):

$$P'(t+\Delta t) = P(t) + V(P,t)\Delta t \#(2)$$

The velocity at the first guess position for the next integration time step is averaged with the initial position's velocity at the current time step to find the true final position for each particle, as shown in equation (3):

$$P(t+\Delta t) = P(t) + 0.5 \times \left[V(P,t) + V(P',t+\Delta t)\right]\Delta t \#(3)$$

A particle can be modeled as a point with a three-dimensional position P suspended within a grid of velocity vectors. At each time step t, a particle first samples the velocity (V(P, t)) in its current position to determine an initial estimated position (P'). The velocity (V(P', t + Δt)) is then sampled at the initial estimated position at the next time step. The average of the two velocities is used to calculate the particle's final position, P'.

This sequence is repeated for a large set of particles defined by the user for each emission source, where the combined concentration of final particle positions at the end of the time step forms the plume distribution. Inter-particle collisions are not considered since each particle is considered in the model framework to be infinitesimally small.

2.3. Ramsdell and Fosmire Plume Meander Model for Nearfield Dispersion (RAF)

Dispersion of radionuclides very close to their release point significantly impacts the order of magnitude of dose to individuals standing just beyond the site boundary. Within the nearfield, the size and geometry of buildings play a crucial role in shaping the emitted plume segment before it transports to the farfield, where horizontal dispersion dominates, and vertical dispersion from building wake and terrain has less of an impact.

Specifically, nearfield ranges are defined in Maccs with the parameter RAFDIST as distances less than 1200 m (0.75 miles) from the initial radionuclide source. This nearfield modeling is only implemented for the built-in Maccs GPM from a point source and not for HYSPLIT PIC modeling (Clayton, 2021). Within this nearfield distance, the increase in dispersion can be attributed to the low- (σ_1) and high-wind speed (σ_2) parameters found using equations (4) and (5),

$$\Delta\sigma_1(x)^2 = 2R\,\Delta\tau_1^2\,T_{\Delta1}^2\left[1-\left(1+\frac{x}{T_{\Delta1}\cdot U}\right)\cdot exp\left(\frac{-x}{T_{\Delta1}\cdot U}\right)\right] \#(4)$$

$$\Delta\sigma_2(x)^2 = 2R\,C_t^2\,\alpha_T^2\,U^2\,A\left[1-\left(1+\frac{x}{\alpha_T\cdot\sqrt{A}}\right)\cdot exp\left(\frac{-x}{\alpha_T\cdot\sqrt{A}}\right)\right] \#(5)$$

where *R* is the background turbulence parameter; $\Delta\tau$ is the turbulence increment parameter; T_Δ is the time scale parameter; C_τ is the high-wind speed turbulence increment coefficient; α_T is the high-wind speed time scale coefficient; *A* is the cross-sectional area of the source building; and *U* the wind speed. The same two equations are used in both crosswind (y) and vertical (z) dimensions with different constant parameter values provided by default in Maccs and is listed in Table 1.

2.4. Radionuclide Source Terms and Weather Conditions

Both reactor designs investigated in this study – the Peach Bottom's BWR and the Idaho National Laboratory (INL) Heat Pipe Design A - employ the existing Peach Bottom Nuclear Generating Station as the site location for release simulation, located at the feedwater from the Susquehanna River in Pennsylvania at 39.75° N and 76.26° W. Peach Bottom is located in a flat region (0.25 km elevation) with no significant terrain features.

The SOARCA analysis for Peach Bottom utilized both MELCOR and Maccs, which were utilized in this study. Source terms from the Peach Bottom General Electric 4016 MWth BWR facility assumed a worst-case unmitigated long-term system blackout, ultimately resulting in catastrophic damage and a release of radionuclides (Bixler et al., 2013). Releases from the facility were modeled as an area source centered at the coordinate located 40 m above the ground, emitting 29 hourly segments, with an initial plume standard deviation of 11.6 m in the Y-direction and

23.3 m in the Z-direction for a total exposure of 96 h (U.S. NRC, 2015). INL Heat Pipe Design A reactor is a heat pipe reactor containing an array of 1134 hexagonally-shaped UO2 fuel pellets, with each fuel element containing a centrally located hole for gas to transfer heat outside the reactor; this reactor operates at a maximum power of 5 MW thermal (Sterbentz et al., 2017). Given that the UO2 has the same nuclear fuel composition as Peach Bottom's BWR, the same radionuclides were tracked for those at Peach Bottom. Simulations in MELCOR of a possible accident scenario using extraordinary reactivity injections beyond normal or projected emergency operating scenarios could not result in any measurable radionuclide release. To establish a conservative estimate that establishes the approximate

level of the radiological consequences of operating this nuclear reactor, the end-of-cycle core activity was defined as the source term inventory and the release fractions from the long-term system blackout in the SOARCA analysis for Peach Bottom described above were used for the release scenario. It should be noted that these release fractions are highly improbable for the INL Heat Pipe Design A reactor due to the many inherent safety design features included.

Furthermore, weather data required for the execution of the atmospheric transport in Maccs is obtained from NOAA's North American Mesoscale Forecast System (NAM) with a 12 km × 12 km horizontal resolution Lambert Conformal grid covering the continental United States over the course of 2021 (NAM, 2023). Maccs' parameters largely mirror those NuScale recommended for their dose-in-place model for a stationary population and effective dose exposure estimation for the initial 96 h following plume arrival and is shown in Tables 2 and 3 (Dudek et al., 2022). The only change applied in this study to NuScale's recommended Maccs parameters is the increase of groundshine shielding from 0.7 to 1.0, providing an unmodified base for results.

2.5. ICRP Publication 60 Effective Dose

The quantification of risk associated with the exposure to radiation emitted from a radionuclide plume is calculated using the ICRP Publication 60 Effective Dose (ED) formula along with the Environmental Protection Agency (EPA) Federal Guidance Report (FGR) 13 internal inhalation and external exposure dose coefficients (ICRP, 1990), (Eckerman et al., 1999). It should be noted that the current regulatory statute requires dose coefficients defined in 10 CFR 20.1003 in accordance with even older publications, ICRP Publication 26 and 30, but is not considered in this study due to its obsolescence (U.S. NRC, 2021). Effective dose (Sv) was calculated for a sex-averaged adult standing along the furthestmost boundary in each radial ring element using equation (6).

$$\text{Effective Dose} = \sum_{T} w_T H_T \ \#(6)$$

where w_T is a dimensionless tissue specific weighting factor tabulated in ICRP Publication 60 and H_T is the tissue specific equivalent doses. . Four pathways were considered for radiation exposure: cloudshine, inhalation, skin deposition, and groundshine. Cloudshine occurs when overhead or surrounding radionuclides in a plume emit radiation that is incident upon the individual's skin, but the particles are not actually deposited upon the skin. Inhalation occurs when aerosol particles are inhaled within the lungs during normal breathing, contributing to internal dose. Groundshine occurs when radionuclides deposited upon the ground emit radiation upwards and incident upon an individual's skin. Skin deposition represents the dose from radionuclides that deposit in a thin layer upon clothing and exposed skin. Each radionuclide simulated has a unique effective dose coefficient for each exposure pathway, which is to obtain the final peak dose.

The output metrics used in this study were the mean and 95th percentile peak dose distributions. These statistical values were obtained by repeatedly simulating the same source term, with a new trial started for every hour every day of the year (8760 trials). The peak dose is isotropic, which was found by finding the maximum dose quantity in all radial directions for the given radial distance. As such, when a mean peak dose at 5 km is given, it should be interpreted as the average highest dose possible for an individual standing within a circular ring with an inner radius of 4 km and an outer radius of 5 km centered on the nuclear facility, simulated using all weather conditions over the 2021 annual year. The

95th percentile peak dose is similar in that the peak dose provided indicates that in 95% of all trials run using the 2021 weather season, the dose at the radial distance is at or lower than the value listed.

The dose criteria for the EPZ boundary were defined similarly to those in the NRC-approved NuScale technical basis for a dynamic scalable EPZ (Dudek et al., 2022). These criteria were specified as the furthest distance to the reactor building where doses do not exceed 1 rem (10 mSv) total effective dose equivalent (TEDE) at mean weather conditions and 5 rem (50 mSv) TEDE at the 95th percentile weather condition, over 96 h following initial release. These criteria do not exceed the regulatory maximums in 10 CFR 100.11, which states that exclusion zones must have a maximum of 25 rem (250 mSv) TEDE over the course of 2 h following initial radiological release. Individual plume release fractions are identical for both scenarios and originate from SOARCA's the Peach Bottom BWR hypothetical long duration system loss of offsite power and blackout scenario resulting in catastrophic damage and a release of radionuclides.

3. Results

Study results demonstrated the technical basis for a scalable EPZ of the Peach Bottom BWR and a conceptual power facility utilizing a single INL Heat Pipe reactor. Under 10 CFR 50.160 (U.S. NRC, 2023) and approved NuScale scalable EPZ, operators of these reactors could apply for a non-standard EPZ radius using the methodology described earlier with Maccs' GPM ATD simulation, as well as an alternative ATD method from HYSPLIT PIC integration. Dispersion and consequence analysis was conducted first using publicly available accident progression timeline and source terms developed in SOARCA for the Peach Bottom BWR as a baseline benchmark of conventional nuclear power plants. INL HPR was then simulated using the exact same weather, location, and siting parameters from SOARCA Peach Bottom BWR with only the initial inventory changed to produce a hypothetical release scenario for analysis. These results altogether permit a comprehensive comparative analysis to determine the eligibility and consequences of using a Lagrangian PIC approach over GPM in delineating EPZ boundaries.

Operation of Maccs was conducted on a Windows 10 computer with an I7-8700T processor and 16 GB of memory. Simulation using GPM ATD took at most 3 h to complete all 8760 trials for either source term. Generation of HYSPLIT weather bounding data required for PIC ATD was conducted on Georgia Institute of Technology computing cluster PACE using 64 cores and a wall clock time of 31.5 h. Simulating the PIC dispersion in Maccs was conducted over the course of four days for each scenario.

3.1. Mean Peak ICRP Publication 60 Effective Dose Distribution

To determine the outer boundary of an EPZ, the risk posed to the surrounding environment was determined by charting the peak dose distribution radially outwards and selecting the point at which the dose falls below accepted thresholds. The mean peak ICRP Publication 60 ED is simulated from the position of the existing Peach Bottom Nuclear Power Plant using the published inventory from SOARCA is given in Figs. 1 and 2, with the mean peak effective doses from 100% end-of-cycle inventory of the INL Heat Pipe Design A reactor given in Figs. 3 and 4. The exact quantity of the initial source term activities is found in Tables 4–12. The release fractions from the long-term system blackout in the SOARCA analysis for Peach Bottom provides a conservative ceiling to the possible dose distribution that could be released from the INL Heat.

Using the mean peak dose, 1 rem (10 mSv) threshold, and linear interpolation between available ring elements, an EPZ drawn for the Peach Bottom facility using NuScale thresholds would result in approximately 38 km (24 mi) EPZ using GPM and 43 km (27 mi) EPZ using PIC ATD model. A facility using INL Heat Pipe releasing 100% of the modeled core inventory would instead place their EPZ at only 0.07 km (0.04 mi) using GPM and 0.89 km (0.55 mi) using the PIC ATD model.

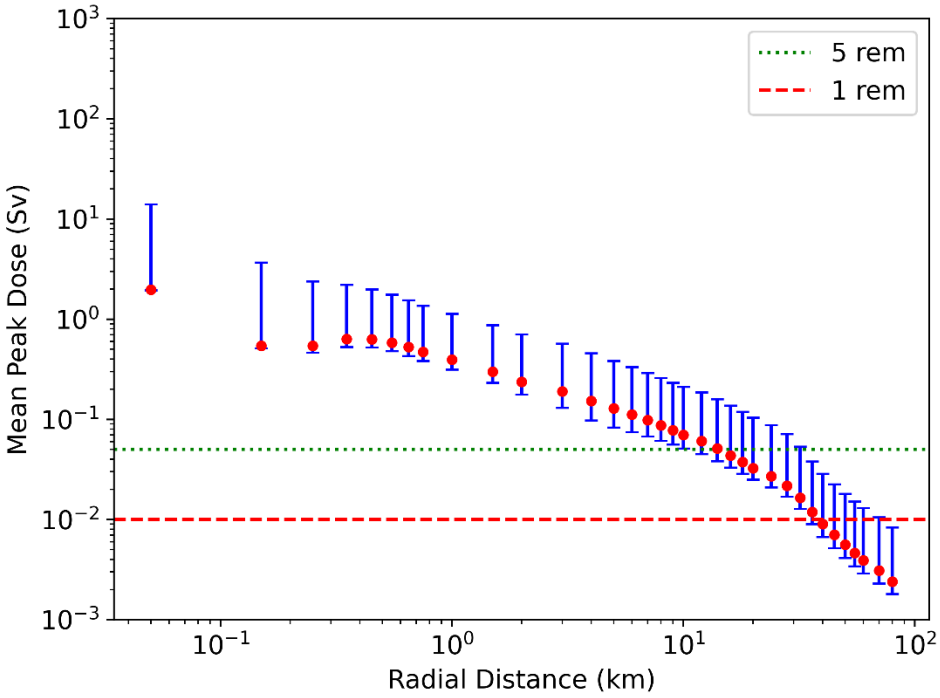

Figure 1: Peak ICRP Publication 60 ED using GPM from SOARCA inventory with 5% and 95% release ranges.

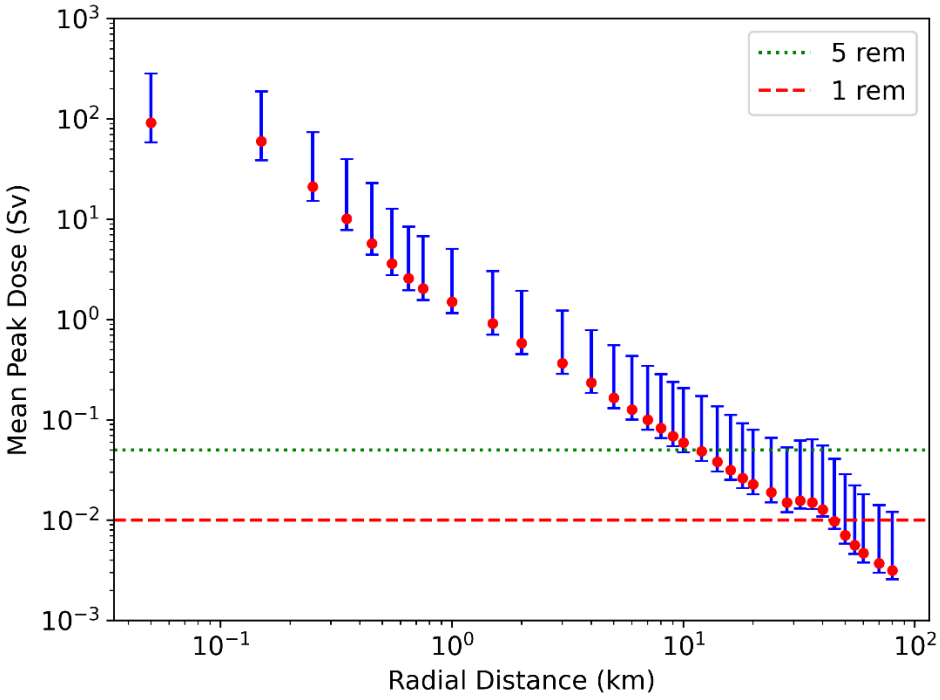

Figure 2: Peak ICRP Publication 60 ED using PIC from SOARCA inventory with 5% and 95% release ranges.

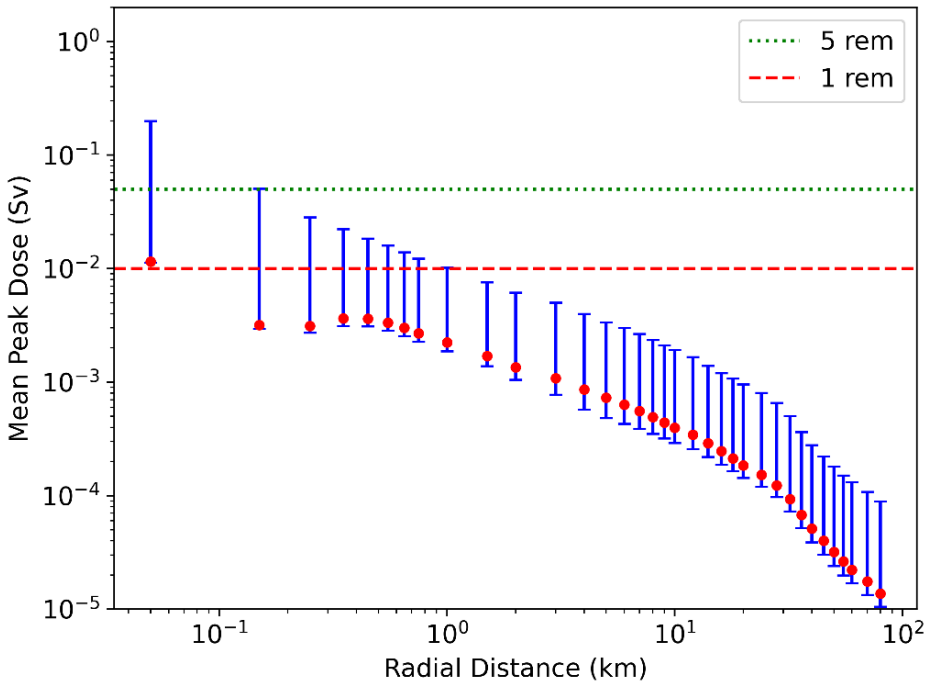

Figure 3: Peak ICRP Publication 60 ED using GPM from INL Heat Pipe end of cycle inventory with 5% and 95% release ranges.

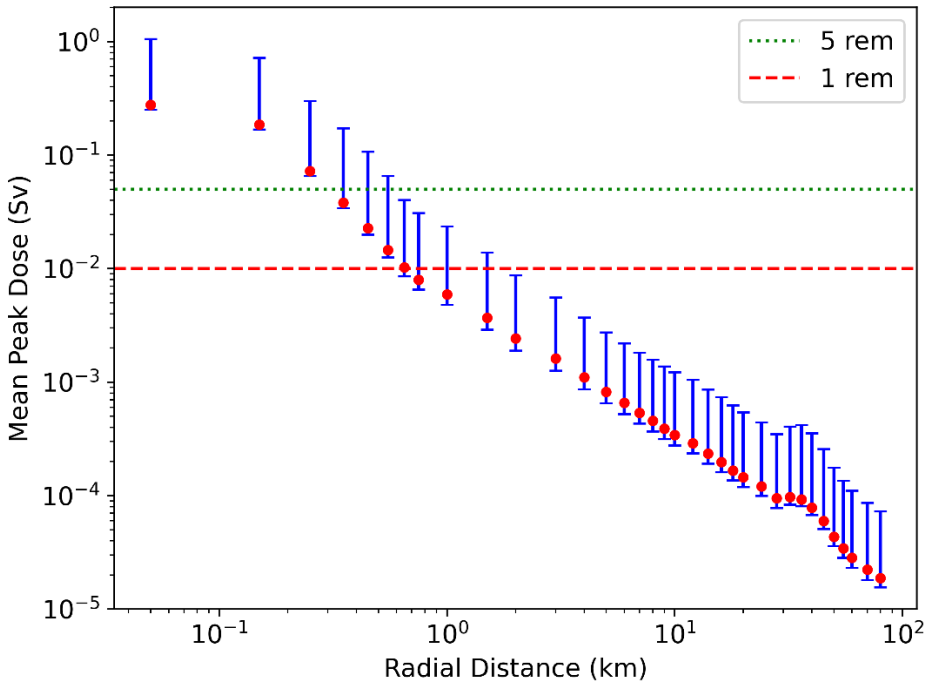

Figure 4: Peak ICRP Publication 60 ED using PIC from INL Heat Pipe end of cycle inventory with 5% and 95% release ranges.

3.2. 95% Weather Peak ICRP Publication 60 Effective Dose Distribution

As safety margin considering a worst-possible realistic weather condition, resulting peak doses where 95% of all simulated trials yielded less than the values graphed are represented as the upper error bars shown in Figs. 1 and 2 for SOARCA Peach Bottom source terms using both GPM and PIC ATD models. The same radionuclide release characteristics, plume size, and duration were simulated for the 100% INL Heat Pipe Design A in Figs. 3 and 4. The EPZ boundary using 95% weather conditions increased the maximum threshold to 5 rem (0.05 Sv) in accordance with NuScale thresholds, where higher safety margins were used for plausible worst-case weather. The EPZ for the Peach Bottom facility using GPM dispersion seen in Figs. 1 and 2 results in an EPZ of 36 km (23 mi), whereas PIC requires 49 km (31 mi). The EPZ for a Heat Pipe reactor using GPM in Fig. 3 would require an EPZ of 0.15 km (0.09 mi), whereas PIC in Fig. 4 requires 0.74 km (0.46 mi). It should be noted that the risk indicated by the higher threshold used to specify the EPZ size using 95% weather conditions could be lower than that with mean conditions; in this case, the largest EPZ size will be selected as the definitive EPZ radius.

3.3. Separated Pathway Contribution to Mean Peak ICRP Publication 60 ED

Mean peak dose values generated using SOARCA Peach Bottom inventories and 100% of INL Heat Pipe reactor end-of-cycle inventory using GPM are presented in Figs. 5 and 7, and using PIC in Figs. 6 and 8, respectively. Exposure pathways were segregated during a single run using the Maccs evacuation cohort functionality. Each evacuation cohort was set to have complete immunity to three pathways using a zero-shielding multiplier, with the last pathway representing total exposure. All trials simulated did not include skin deposition, as Maccs yielded negligible doses at all distances from this pathway.

One noticeable difference between dose distributions estimated by GPM and PIC ATD models was the significant reduction in inhalation dose within the regions closest to the site boundary in GPM results in Figs. 5 and 7 that is not present in PIC estimates of Figs. 6 and 8. A plume originating 40 m above the ground did not immediately drop to the ground where an individual could inhale the plume. GPM inherently accounts for this in the vertical dimension with a Gaussian normal-shaped dispersion that increased radially outwards such that the plume would require transport over a certain distance before reaching the ground.

In all scenarios, the dominant source of exposure dose originated from the groundshine pathway, with inhalation contributing less than half the total dose and cloudshine in the single-digit percentages. The sum of all pathways forms the depicted mean peak ICRP Publication 60 Effective Dose given in Figs. 1–4. Figs. 5–8 parse the individual dose pathways, with the upper line of groundshine dose equaling the mean peak dose in their respective figures.

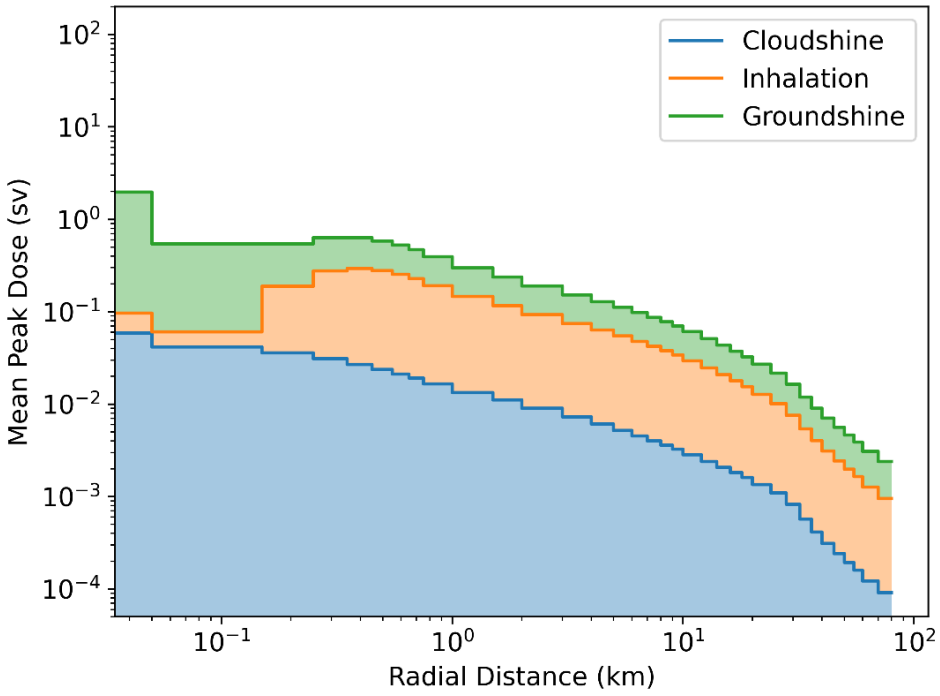

Figure 5: GPM separated total mean peak ICRP Publication 60 ED pathways using SOARCA inventories.

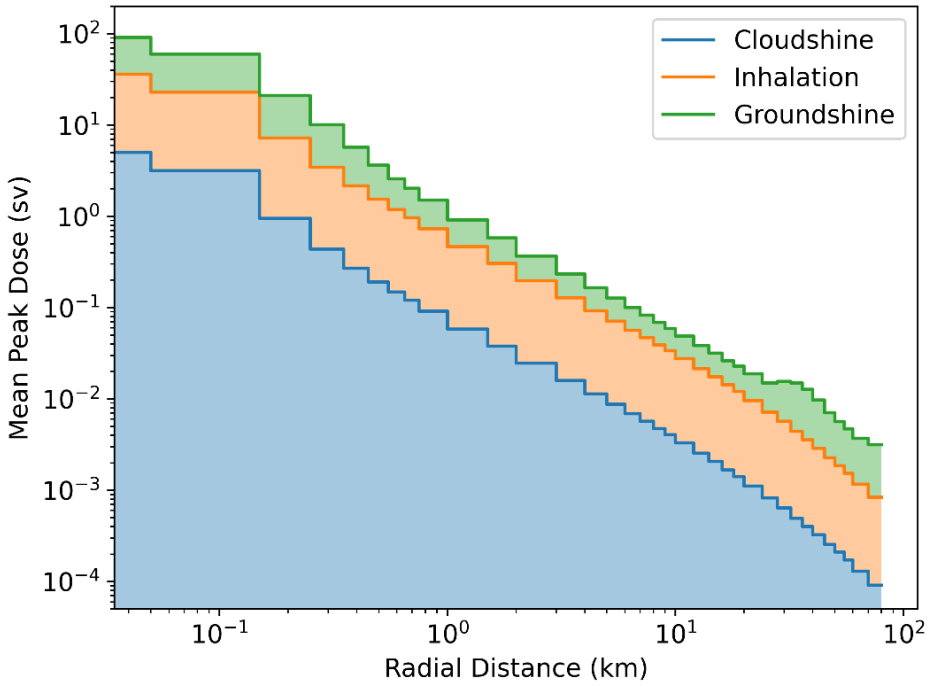

Figure 6: PIC separated pathways from SOARCA release to total mean peak ICRP Publication 60 ED.

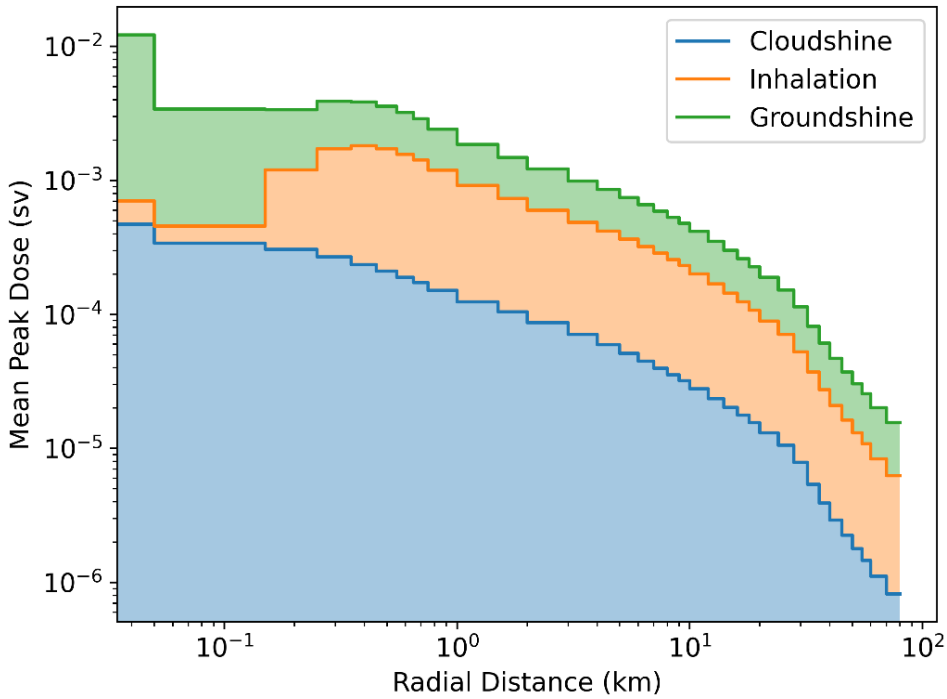

Figure 7: GPM separated pathways from INL Heat Pipe release to total mean peak ICRP Publication 60 ED.

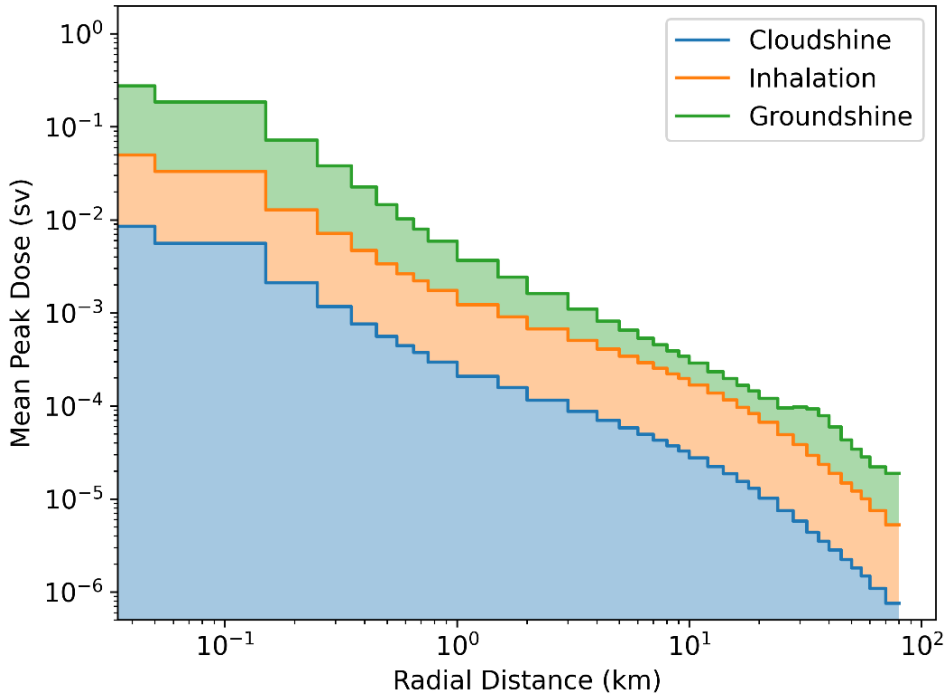

Figure 8: PIC separated pathways from INL Heat Pipe release to total mean peak ICRP Publication 60 ED.

3.4. GPM With and Without RAF Meander Modeling

Additional simulation of the SOARCA Peach Bottom demonstrating the impact of RAF was further examined. In Figs. 9 and 10, the vertical line drawn demonstrates the 1.2 km radial distance that divides the nearfield where the RAF meander model actively influences the dispersion factors of the Gaussian plume and farfield where it is inactive. In both figures, ratios above unity indicate that the mean peak doses from the simulation without RAF influences are higher than those with RAF. The primary source of the lower dose observed is due to the changes in the groundshine dose since it is the dominant dose pathway. When using the RAF model, the nearfield dispersion was increased, resulting in lower ground-level air concentrations and lower ground deposition.

However, while the effect of RAF meandering halves the nearfield doses, at most, arbitrarily applying the resulting RAF meander model's GPM radial ratios onto the HYSPLIT PIC distribution does not significantly affect the calculated nearfield doses. A dedicated PIC nearfield model would need approximately two orders of magnitude reduction to bring HYSPLIT in line with the estimations that GPM generates for the same radial distances using RAF modeling. Specialized nearfield handling of PIC particles is thus required to correctly simulate the plume dispersion and dose distribution when accounting for building and other low-level obstacle wakes.

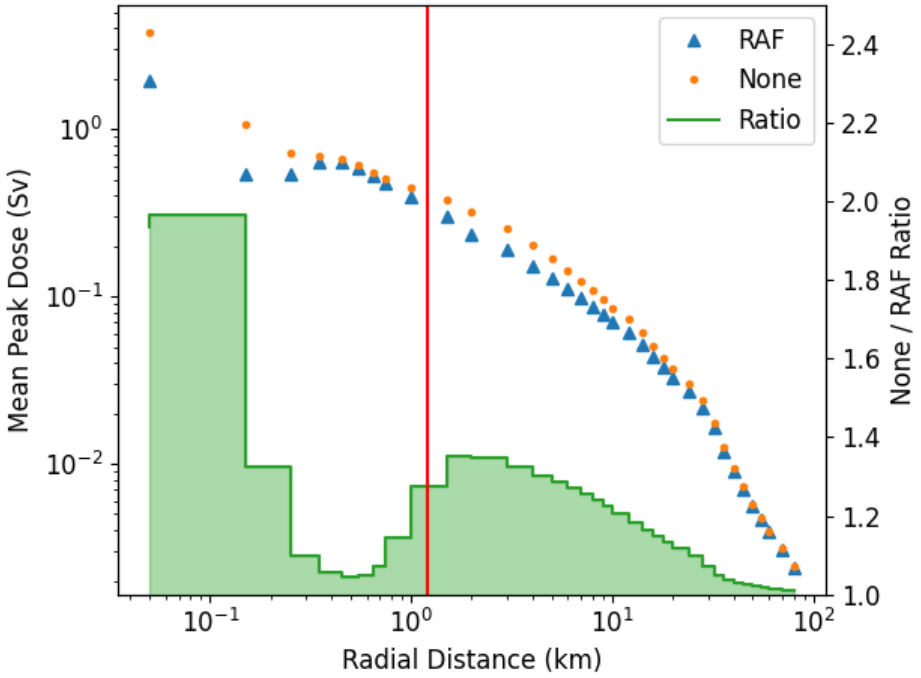

Figure 9: GPM mean peak ICRP Publication 60 ED and ratio with and without RAF meander modeling using SOARCA release inventory.

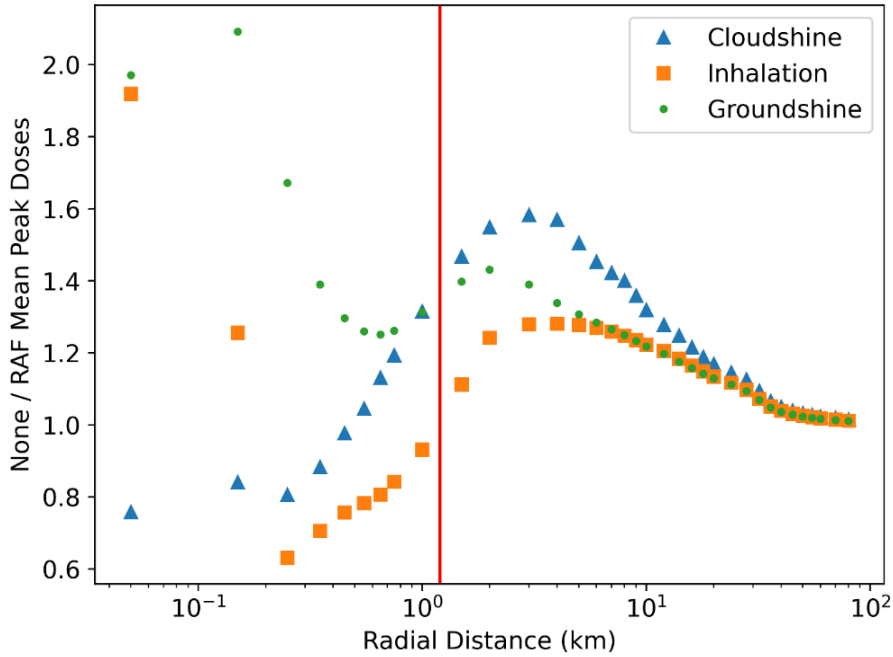

Figure 10: Ratio between without and with RAF meander modeling for GPM dispersal of SOARCA release inventory.

3.5. HYSPLIT NOAA Weather Data Resolution

Another consideration when using the PIC HYSPLIT model is the grid square size of the underlying weather data. From most coarse to finest available resolutions, Fig. 11 used GDAS1 1-degree (120 km) gridded data, Fig. 12 used GFS 0.25-degree (30 km) gridded data, Fig. 13 used NAM12 12 km gridded data, and Fig. 14 used HRRR 3 km gridded data. All previous GPM and PIC mode simulations sourced weather files from NAM12 (NAM, 2023); a 12 km gridded data set is displayed in Fig. 13.

The results in Figs. 11–14 employ a HYSPLIT PIC simulation using one unit mass dispersion over 24 h with continuous uniform release of the unit mass during the entire period. With a constant core radionuclide release inventory, the mass is directly proportional to the dose rate experienced at a location. Furthermore, given the relatively short simulation period, more than one day is needed to disperse the inventory fully, and the maximum point of concentration will be close to the source in the nearfield. Thus, the maximum concentration order of magnitude does not change when varying weather grid resolution. Hence, the significantly high estimate of doses in the nearfield would not significantly change.

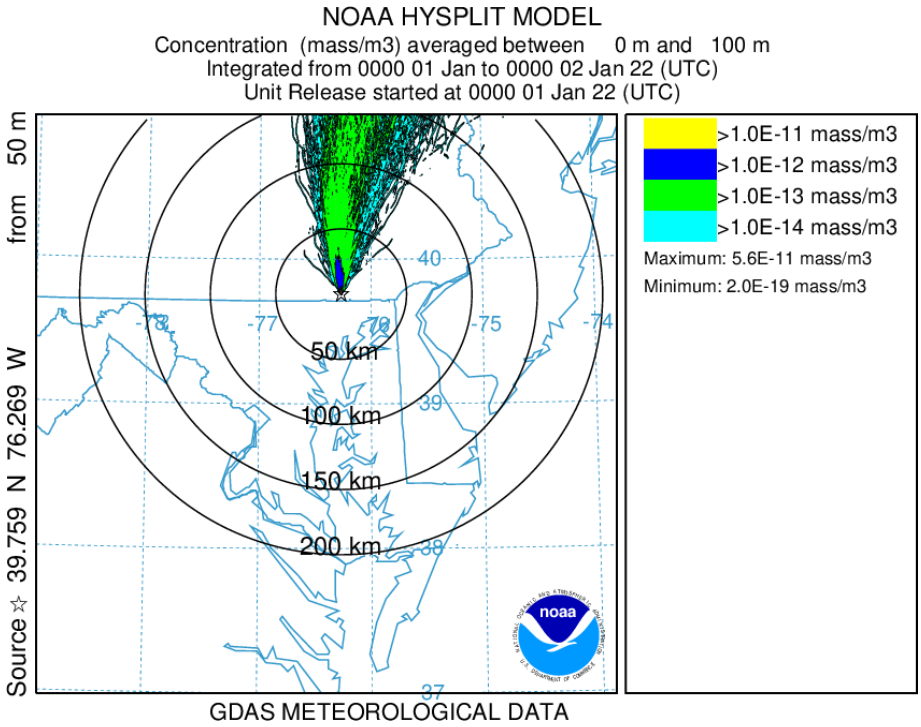

Figure 11: HYSPLIT atmospheric dispersion simulated using unit mass with global GDAS1 1-degree (120 km) data resolution.

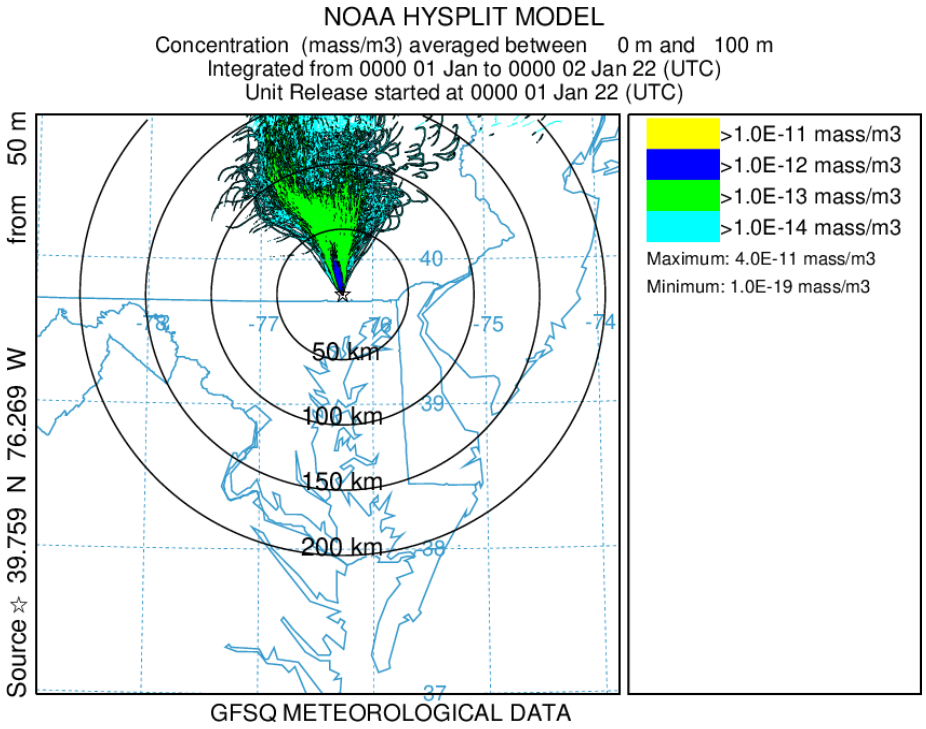

Figure 12: HYSPLIT atmospheric dispersion simulated using unit mass with global GFS0p25 0.25-degree (30 km) data resolution.

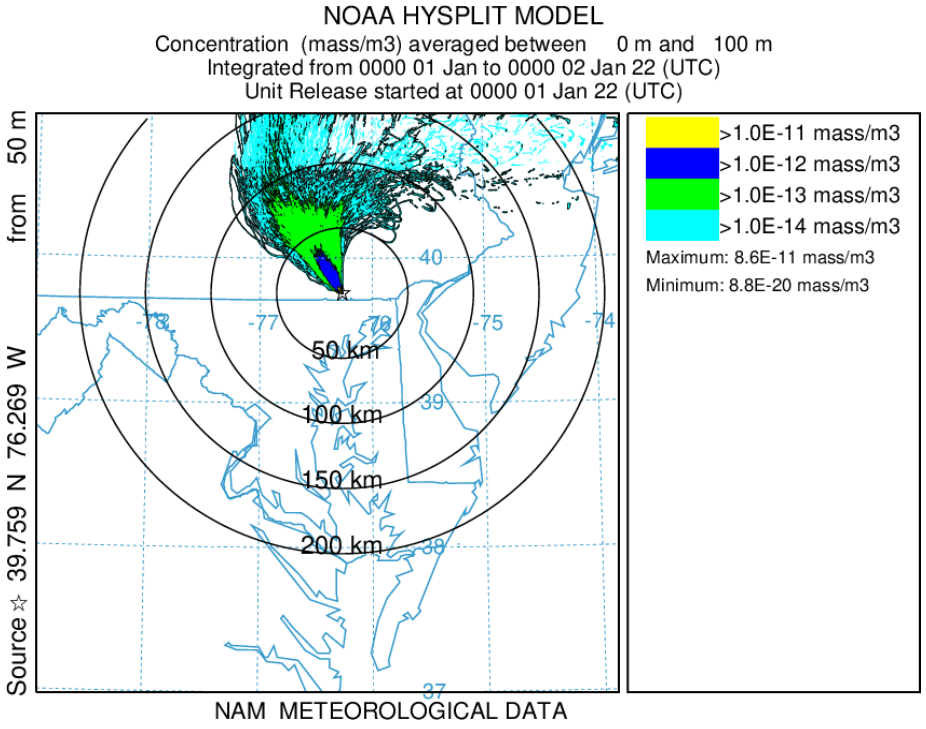

Figure 13: HYSPLIT atmospheric dispersion simulated using unit mass with continental NAM12 12 km data resolution currently used in this study for PIC results.

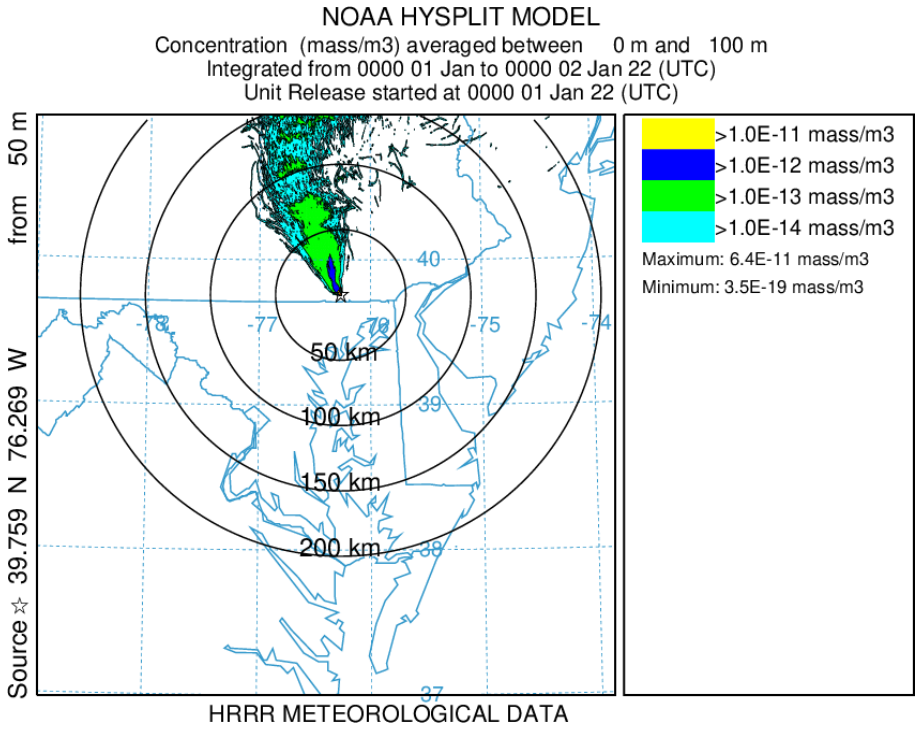

Figure 14: HYSPLIT atmospheric dispersion simulated using unit mass with continental HRRR 3 km data resolution.

3.6 Isotope Class Contribution to Mean Peak Dose

Individual radionuclide contributions to the mean peak dose were obtained in Maccs by setting all inventories, other than the radionuclide class of interest, to zero activity and running the simulation where all other inputs remained the same. Radionuclides were selected and grouped in accordance with SOARCA radionuclide classes, as detailed in Tables 4–12. Fig. 15 displays the contribution to mean peak ICRP Publication 60 Effective Dose by radionuclide class from INL Heat Pipe inventory for the GPM results. The highest three contributing groups, alkaline earths, iodine, and chalcogens, are charted in Fig. 16, Fig. 18, and Fig. 20 for GPM and Fig. 17, Fig. 19, and Fig. 21 for PIC by pathway. For split contribution charts, values are displayed in an additive stacked format such that the uppermost value, chalcogens in all cases, is approximately equal to the respective pathway contribution found in Figs. 7 and 8. The difference results from not including the other radionuclide classes that are an order of magnitude less than the highest three contributors found in Fig. 15.

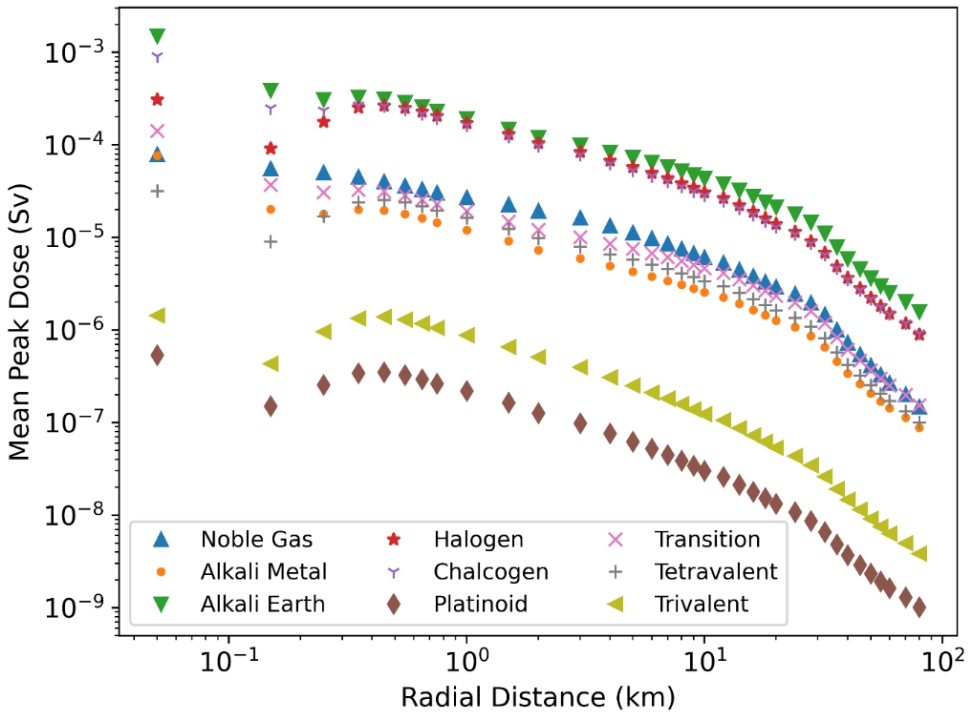

Figure 15: GPM mean peak ICRP Publication 60 ED by radionuclide class from INL Heat Pipe inventory.

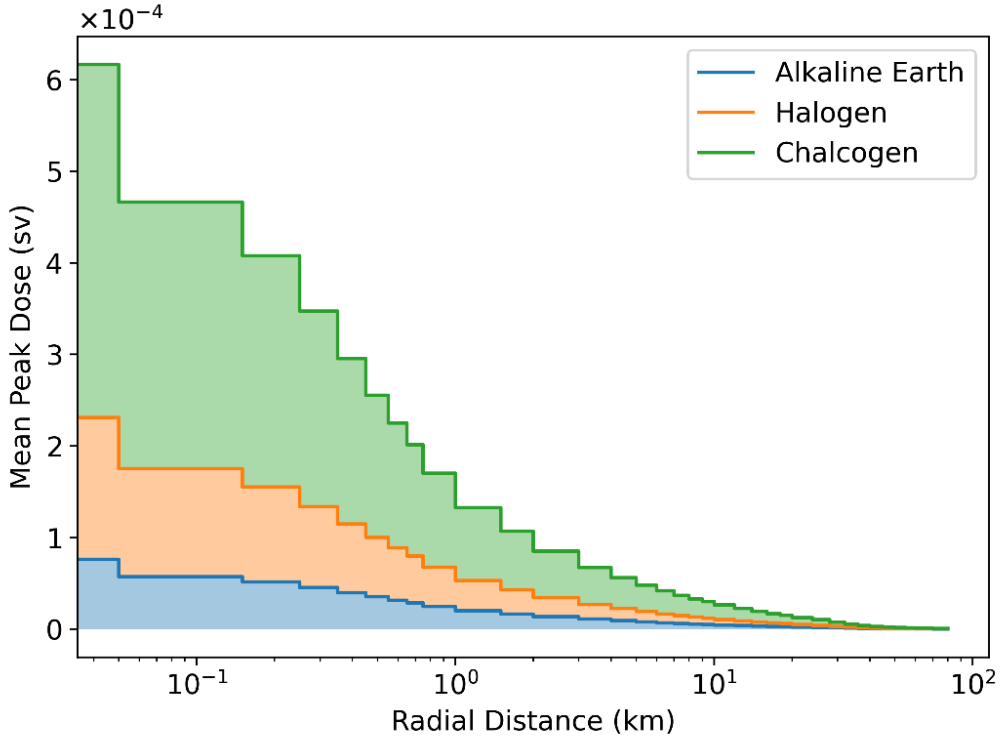

Figure 16: GPM mean peak dose from cloudshine using INL Heat Pipe inventory.

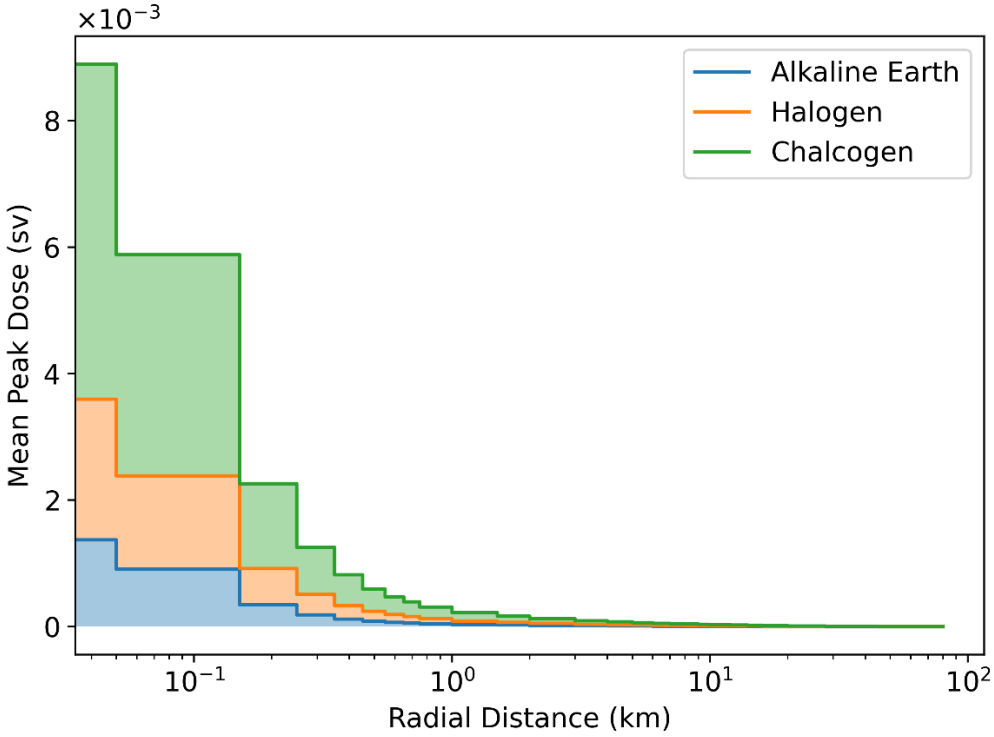

Figure 17: PIC mean peak dose from cloudshine using INL Heat Pipe inventory.

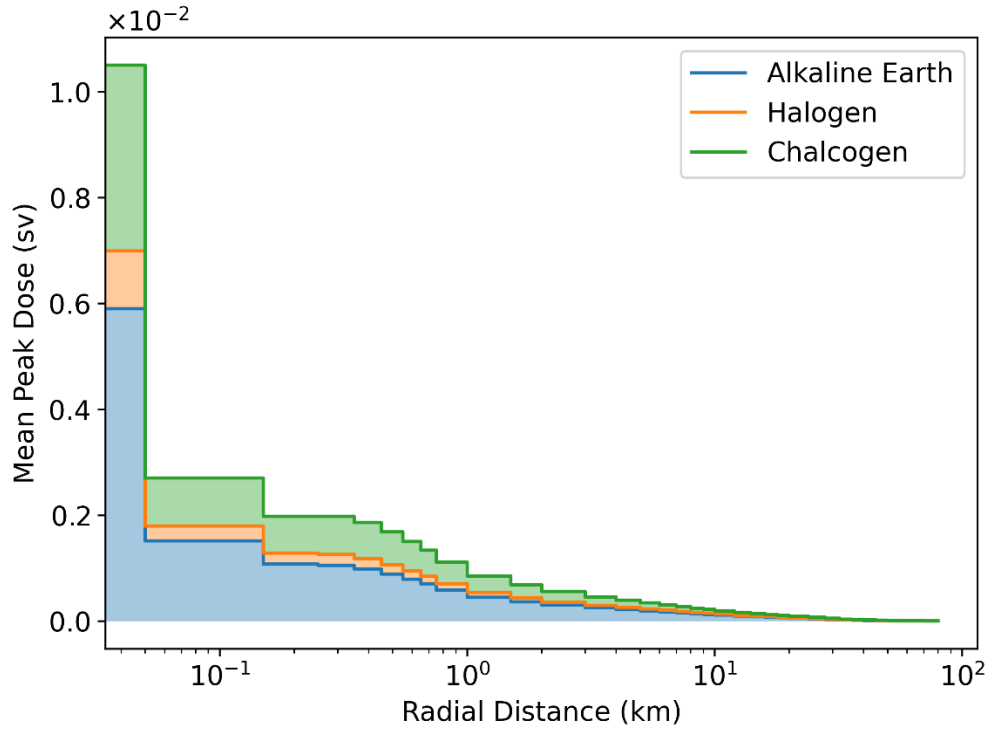

Figure 18: GPM mean peak dose from groundshine using INL Heat Pipe inventory.

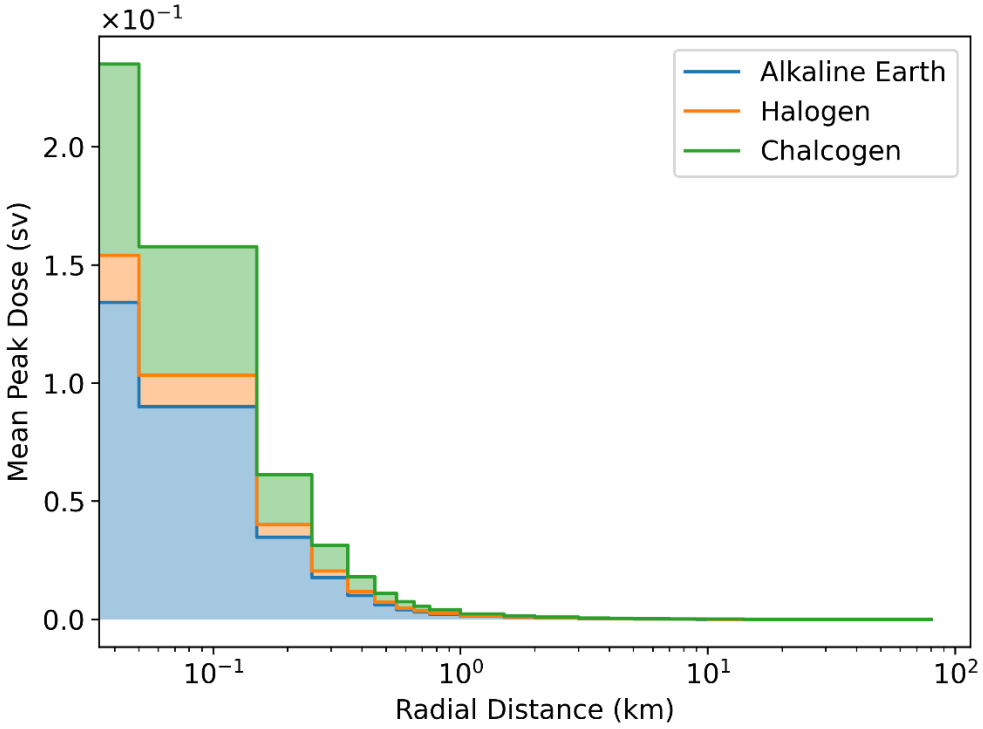

Figure 19: PIC mean peak dose from groundshine using INL Heat Pipe inventory.

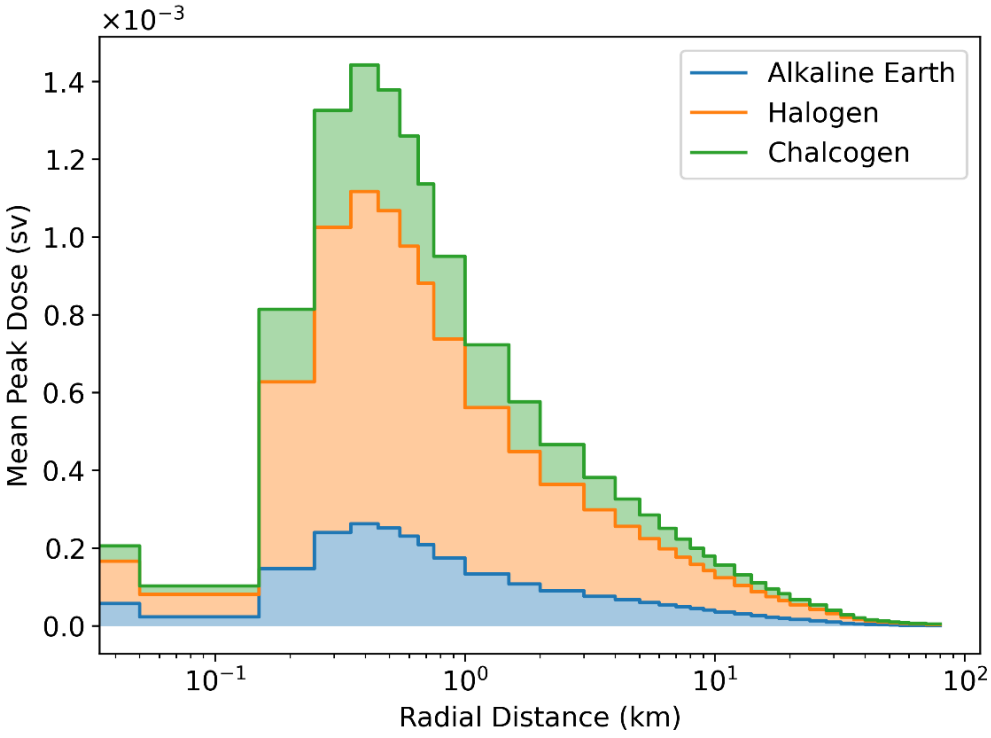

Figure 20: GPM mean peak dose from inhalation using INL Heat Pipe inventory.

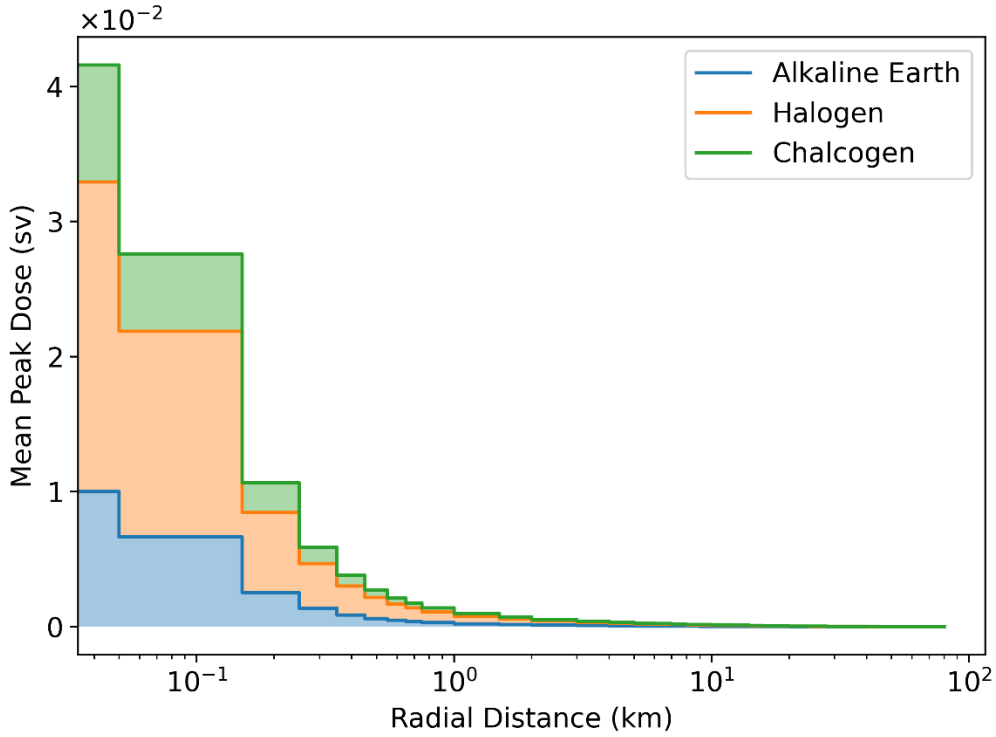

Figure 21: PIC mean peak dose from inhalation using INL Heat Pipe inventory.

4. Discussion

4.1. ICRP Publication 60 ED Peak Dose Distribution

When comparing the results from SOARCA and INL Heat Pipe inventories, a sharp uptick between GPM and PIC dose distribution at around 30 km was observed. This is mirrored in the similar behavior of a sharp increase in groundshine dose rate in Fig. 6. While Maccs does not have any ability to investigate the source of greater deposition that results in higher groundshine doses, one explanation of these results can be derived by analyzing the map surrounding the Peach Bottom facility, almost precisely at the start of the peak at 30 km sits the coastline of the Chesapeake Bay whose waters may induce higher deposition of particulates due to the greater humidity and cloud cover. The straight-line Gaussian model implemented into Maccs is only aware of the weather conditions and ground surface roughness at the release point and not any downwind. Hence, prominent geographical features like a body of water, which drastically alters the weather conditions above it, and ground surface roughness for deposition purposes cannot be accounted for in the GPM deposition functions and can be a significant source of inaccuracy as distance increases from the source position. HYSPLIT PIC does not have this limitation, as particles continuously sample the weather and ground surface roughness at their current grid position as the simulation progresses.

The comparison between GPM and PIC inhalation dose contribution in Figs. 20 and 21, respectively, highlights a significant reduction of mean peak dose in the nearfield within 0.6 km for GPM. This results from GPM's theoretical basis, which involves a vertical Gaussian normal distribution centered at the release height and extending outward using tabulated standard deviation dispersion. Similar to a

chimney, the plume of particulates requires some distance and vertical dispersion for most radionuclide aerosols to reach the ground and for individuals standing at each radial bin element to breathe in the contaminated air actively. At a release height of 40 m, the GPM estimates that an average individual standing close to the site boundary remains breathing in a small envelope of clean air and not contributing to the inhalation dose measured at the nearfield distance. However, HYSPLIT's PIC does not model this effect and instead has higher inhalation doses for those standing in the nearfield.

4.2. EPZ Radius

As the final EPZ would be the greatest value between both mean peak dose and 95% weather conditions peak dose, the final EPZs of the Peach Bottom BWR reactor would be 38 km (24 mi) using GPM atmospheric modeling and 49 km (31 mi) using PIC; both of which is significantly larger and more conservative than the existing 10-mile EPZ regulatory requirement under 10 CFR 50.47 for plume exposure from design basis accidents (U.S. NRC, 2013). The larger distance is due to the larger source modeled in this study compared with design basis accidents. On the other hand, an INL Heat Pipe reactor requires 0.15 km (0.09 mi) using GPM from 95% weather conditions and 0.89 km (0.55 mi) using the PIC ATD model at mean weather conditions assuming that the entire core inventory, both fuel and byproducts, managed to be ground into fine enough particulates to be lofted into a plume.

Plume release fractions remain unchanged between SOARCA Peach Bottom and INL Heat Pipe Reactor scenarios. This means that all conditions obtained during the accident developed in SOARCA to encompass the long-term loss of offsite power at Peach Bottom Nuclear Generating Station is assumed to have occurred with the only difference that the core was replaced by INL Heat Pipe Reactor design. This is a conservative estimation of a maximum hypothetical bounding accident that may occur as the conditions and assumptions used to develop the plume progression and duration within the facility were on a large conventional BWR and does not take into account the passive safety designed into the HPR. Under these conditions, the INL Heat Pipe Reactor EPZ is significantly smaller than the current 10 CFR 50.47 regulatory requirements of 10-miles. It would still require offsite emergency planning when this maximum hypothetical accident is used as the basis for an EPZ sizing under 10 CFR 50.160. An operator of a microreactor should consider a more in-depth assessment using the conditions and risk for a facility built around one or more ARs that will more appropriately size the EPZ.

4.3. Impact of RAF Meander Modeling on GPM Dispersion in the Nearfield

Nearfield distances were defined by a parameter in Maccs as 1.2 km (0.75 miles). Within this range for the GPM atmospheric transport, RAF empirical functions enhance the standard deviations to represent the effect of buildings and wind speed on plume dispersal. When applied to the Gaussian model, as seen in Fig. 9, the final distribution of mean peak doses was suppressed by up to half the original amount, with a greater proportion of reduction being applied to the groundshine exposure from deposited radionuclides near the site boundary.

Using the RAF plume meander model yields subsequent mean peak ICRP Publication 60 ED distribution lower than without implementation, including beyond the 1.2 km cutoff where RAF no longer actively affects the plume dispersion. Increased nearfield dispersion resulted in lower exposure in the farfield, which decreased with distance. In both Figs. 9 and 10, ratios greater than unity indicated decreased individual radiation exposure dose when applying the RAF meander model to the Gaussian plume in the nearfield. Fig. 10 demonstrates that the predominant dose reduction resulting from using RAF meandering in the nearfield emerges from increasing plume dispersion in the horizontal and vertical

directions, thereby decreasing the source exposure concentration of radionuclides. However, RAF meander modeling only applies to a Gaussian plume model; even when applying an upper ratio of a uniform one-half reduction in dose using RAF modeling in the HYSPLIT PIC simulation, the two orders of magnitude difference in the nearfield radial bins' mean peak dose cannot be discounted.

4.4. HYSPLIT NOAA Weather Data Resolution

Recent advancements have suggested potential solutions for improving particle dispersion in the nearfield and mitigating the risks of high concentration levels. This is a promising approach derived from investigating alternative weather data sources to be utilized in the HYSPLIT system. The proposed solution for addressing the issue of particles clumping near the source involves the implementation of additional wind vectors or sampling options that facilitate the grouping of particles. This approach aims to simulate the original dispersion effect observed in the plume meander model and GPM findings.

Unfortunately, this was not evident when simulating preliminary results using all four available archived weather data from NOAA. Using the maximum concentration that was recorded from a release of a unit mass over the course of a day, where deviations were present, but all remained in the same order of magnitude as the reference NAM12 weather database used for all PIC models (NAM, 2023). Given that the peak dose observed was found to be directly proportional to the radionuclide activity released from the reactor, this finding suggests that the issue of high particle concentration persisted across all four separate resolutions, irrespective of the weather format utilized in simulating particle tracks via HYSPLIT. It should be noted that the finest available grid resolution, 3 km for using the high resolution rapid refresh (HRRR) model, does not resolve building wake effects or other low-altitude wind conditions that may increase nearfield particle dispersion.

This result was replicated in a sensitivity study conducted in the same Maccs HYSPLIT benchmark to confirm the validity of HYSPLIT in farfield conditions and even beyond in the hundreds of kilometers. Using NAM12 or an alternative weather source WRF27, in which weather data was defined by a grid of 27 km × 27 km elements, the radial peak doses in both GPM and PIC modes when compared to NAM12 produced on average ratios close to unity for a site similar to Peach Bottom which indicates no significant impact on using a coarser grid to simulate the particle tracks and distribution in HYSPLIT that could address the differences in nearfield dose (Clayton et al., 2022).

4.5 Isotope Class Contribution to Mean Peak Dose

Maccs models groups of radionuclides with similar physical characteristics, such as particle size and resulting deposition velocity (Leute et al., 2021). As such, it is possible to individually isolate groups of radionuclides into classes as done in Figs. 15–21; all figures assumed an INL Heat Pipe reactor at the end-of-cycle with 100% release as the inventory. The subsequent contribution to the mean peak dose is a function of each radionuclide's FGR 13 dose coefficients.

For both cloudshine and groundshine dose distributions, the general trend of high dose closest to the release point was mirrored across both GPM and PIC results, with the difference being the magnitude of the first two radial bin segments; PIC simulated an order of magnitude greater mean peak dose closest to the site boundary compared to GPM. However, the most significant difference was found when comparing the inhalation dose contribution simulated with GPM and PIC in Figs. 20 and 21, respectively. The lack of increased dispersion in the nearfield and immediate exposure to radionuclides results in PIC attributing a significant dose to an individual in the nearfield to inhalation. In comparison, GPM plume

expansion requires distance before an individual on the ground can inhale radionuclides, as seen in the lack of inhalation dose for the first two radial bin elements.

5. Conclusion

To investigate the utilization of dose-based siting boundaries for AR EPZ regulatory siting, a comparison of GPM in Maccs and Lagrangian PIC HYSPLIT ATD models was conducted. The difference in assumptions used when modeling ATD significantly impacted EPZ radii when a threshold requirement was used, especially in cases where the simulated source term was small and plumes existed only in significant concentrations at the nearfield ranges.

A comparison conducted in the nearfield revealed a challenging issue for operators of advanced nuclear reactors, particularly small or microreactors that generate proportionally smaller source terms whose plumes dissipate to low concentrations within the nearfield distances. It has been observed that a difference of several orders of magnitude within the nearfield could result in an EPZ encompassing a region close to or even at site boundaries when compared against a larger EPZ found using the PIC ATD model. Limitations in the grid resolution of HYSPLIT in Maccs, in its current implementation, were determined to be too coarse to accurately evaluate nearfield dispersion, which is highly relevant to AR siting locations.

For large source terms, such as the one developed in SOARCA for the Peach Bottom BWR used in this study, the plume segments would extend deep into the farfield, where the GPM and PIC results strongly converge. However, NuScale's risk-informed approach for design basis accidents, when applied to large BWRs, still requires an EPZ with an area at least

5.6 times greater than existing regulations in 10 CFR 50.47 (U.S. NRC, 2013). Therefore, operators seeking to apply a scalable EPZ radius to their facility should only use ARs whose enhanced safety produces minimal source terms that can provide an even greater safety margin with a reduced EPZ radius than existing regulations. For a microreactor source term, such as the INL Heat Pipe reactor, study results demonstrated that HYSPLIT PIC modeling resulted in prohibitively high dose distributions compared to estimates from existing Gaussian ATD models. This emerges from model implementation that results in a combined order of magnitude difference in dose contributed by all dose pathways and in particular inhalation mean peak dose at distances closest to the site boundary. In this nearfield approximation, only GPM with plume meander adjustments should be consulted for dose estimations. This is of particular interest in the context of the small source term obtained from the INL Heat Pipe reactor design when using the conservative PIC estimate, as it will necessitate a larger offsite EPZ compared to GPM. Further investigation of AR concepts with larger core inventories is needed to validate a technology-neutral scalable EPZ methodology.

In the nearfield, only the GPM is recommended to estimate the peak dose for individuals in this region as only GPM has been validated for use within and immediately outside the nearfield and in the farfield; a combination of GPM and PIC is recommended to confirm risk estimations. For situations where a plume needs to be transported in specific weather conditions, a HYSPLIT PIC simulation is recommended, as it can properly adjust the speed and direction of modeled particulates for atmospheric conditions beyond the initial point of release. As only one site was evaluated as a case in this study, a sensitivity analysis of the suitability of GPM and PIC for alternative sites with variable topological features (e.g., near mountains or coast) or extreme weather conditions (e.g., U.S. Gulf Coast)

is recommended for future work, representing scenarios of greater dispersion and non-Gaussian behavior of plumes within the simulated region.

Overall, study results concluded that the new Lagrangian HYSPLIT PIC mode in Maccs suggests that the straight-line Gaussian approximation remains suitable for nearfield plume dispersion and risk estimation. Nuclear power plant operators and regulators should continue to evaluate the utility of Lagrangian PIC into Maccs for improved nearfield modeling to inform the establishment of siting boundaries in AR licensing.

6. Acknowledgement

This work was funded by the Department of Energy – Nuclear Energy University Programs under prime award DE-NE0009135 (Contract M2201185-28-520490-00002 with Texas A&M University and Georgia Institute of Technology). The authors would like to thank Dr. Karen Vierow Kirkland and Thomas Freyman at Texas A&M University, and Chris Faucett, Steven Horowitz, Alan Evans, and Jennifer Leute at Sandia National Laboratories, for their support in actuating this work.

7. References

Bixler, N., Gauntt, R., Jones, J., Leonard, M., 2013. Peach Bottom Integrated Analysis. In: State-of-the-Art Reactor Consequence Analyses Project, Volume 1. Sandia National Laboratories.

Carless, T.S., Talabi, S.M., Fischbeck, P.S., 2019. Risk and Regulatory Considerations for Small Modular Reactor Emergency Planning Zones based on Passive Decontamination Potential. Energy 167, 740–756. https://doi.org/10.1016/j. energy.2018.10.173.

Clayton, D.J., 2021. Implementation of Additional Models into the Maccs Code for Nearfield Consequence Analysis. Sandia National Laboratories.

Clayton, D.J., Bixler, N.E., Compton, K.L., 2022. HYSPLIT/Maccs Atmospheric Dispersion Model Technical Documentation and Benchmark Analysis. Sandia National Laboratories.

Doane, M.M., 2022. Population-Related Siting Considerations for Advanced Reactors. U.S. Nuclear Regulatory Commission.

Draxler, R.R., Hess, G.D., 1998. An overview of the HYSPLIT_4 modelling system for trajectories, dispersion, and deposition. Aust. Meteorol. Mag. 47, 295–308.

Dudek, M., Tesfaye, G., Bavol, B., Schiller, A., 2022. “NuScale Power, LLC Submittal of the Approved Version of NuScale Topical Report, ‘Methodology for Establishing the Technical Basis for Plume Exposure Emergency Planning Zones at NuScale Small Modular Reactor Plant Sites,’ ”. U.S. Nuclear Regulatory Commission. TR-0915-17772-P-A, Revision 3.

Eckerman, K.F., Leggett, R.W., Nelson, C.B., Puskin, J.S., Richardson, A.C.B., 1999. Federal Guidance Report No. 13: Cancer Risk Coefficients for Environmental Exposure to Radionuclides. Oak Ridge National Laboratory, Oak Ridge, TN.

Idaho National Laboratory, 2010. Determining the Appropriate Emergency Planning Zone Size and Emergency Planning Attributes for an HTGR. Idaho National Laboratory. INL/MIS-10-19799.

International Atomic Energy Agency, 2013. Actions to Protect the Public in an Emergency Due to Severe Conditions at a Light Water Reactor. International Atomic Energy Agency.

International Commission on Radiological Protection, 1990. ICRP Publication 60:1990 Recommendations of the International Commission on Radiological Protection. International Commission on Radiological Protection.

Leute, J., Walton, F., Mitchell, R., 2021. Maccs (MELCOR Accident Consequence Code System) User Guide – Version 4.0. Sandia National Laboratories, Albuquerque, NM.

Maioli, A., 2009. Revising the EPZ for IRIS. Westinghouse Electric Company LLC.

Moe, W.L., 2014. Opportunities in SMR Emergency Planning. Idaho National Laboratory.

National Centers for Environmental Prediction, 2023. "North American Mesoscale Forecast System (NAM) [12 Km]." ftp://arlftp.arlhq.noaa.gov/archives/nam12. National Centers for Environmental Prediction, Last accessed May 2023.

Nosek, A., Bixler, N., 2021. Maccs Theory Manual. Sandia National Laboratories.

Ramana, M.V., Hopkins, L.B., Glaser, A., 2013. Licensing small modular reactors. Energy 61, 555–564. https://doi.org/10.1016/j.energy.2013.09.010.

Ramsdell, J.V., 1988. Atmospheric Diffusion for Control Room Habitability Assessments. Pacific Northwest Laboratories.

Satorius, M.A., 2015. Options for Emergency Preparedness for Small Modular Reactors and Other New Technologies. U.S. Nuclear Regulatory Commission.

Sterbentz, J.W., et al., 2017. Preliminary Assessment of Two Alternative Core Design Concepts for the Special Purpose Reactor. Idaho National Laboratory. https://doi. org/10.2172/1413987.

U.S. Nuclear Regulatory Commission, 1977. Regulatory Guide 1.111: Methods for Estimating Atmospheric Transport and Dispersion of Gaseous Effluents in Routine Releases from Light-Water-Cooled Reactors. U.S. Nuclear Regulatory Commission.

U.S. Nuclear Regulatory Commission, 1979. Regulatory Guide 1.145: Atmospheric Dispersion Models for Potential Accident Consequence Assessments at Nuclear Power Plants. U.S. Nuclear Regulatory Commission.

U.S. Nuclear Regulatory Commission, 2013. Emergency Plans. 10 C.F.R. 50.47. U.S. Nuclear Regulatory Commission.

U.S. Nuclear Regulatory Commission, 2015 SOARCA Source Term Files.https://www. nrc.gov/docs/ML1505/ML15054A210.html.

U.S. Nuclear Regulatory Commission, 2020. Emergency Preparedness for Small Modular Reactors and Other New Technologies, 10 CFR 50.160.

U.S. Nuclear Regulatory Commission, 2020. Regulatory Analysis for the Proposed Rule: Emergency Preparedness for Small Modular Reactors and Other New Technologies. U.S. Nuclear Regulatory Commission. ML18134A086.

U.S. Nuclear Regulatory Commission. 2021. Definitions. Nuclear Regulatory Commission. 10 C.F.R. 20.1003.

U.S. Nuclear Regulatory Commission, 2021. Preliminary Rule Language Subpart F - Requirements for Operations, Section 53.820 - Emergency Preparedness. U.S. Nuclear Regulatory Commission. ML21145A028.

Wang, J., Clayton, D., Dewji, S.A., 2023. Risk-informed comparison of atmospheric plume models for dose-based advanced reactor licensing siting. American Nuclear Society 18th International Probabilistic Safety Assessment and Analysis (PSA 2023). https://doi.org/10.13182/PSA23-41458.

Wiggins, J.T., Johnson, M.R., 2011. Development of an Emergency Planning and Preparedness Framework for Small Modular Reactors. U.S. Nuclear Regulatory Commission. SECY-11-0152.

8. Tables

Table 1: Maccs Ramsdell and Fosmire Plume Meander Model Parameters [21], [30]

Parameter	Value	Unit	Parameter	Value	Unit
R_x	0.655	-----	R_y	0.584	----
$\Delta\tau_{x1}$	0.835	m/s	$\Delta\tau_{y1}$	0.239	m/s
$T_{\Delta x1}$	1,000	s	$T_{\Delta y1}$	100	s
$C_{\tau x}$	0.02	s/m	$C_{\tau y}$	0.01	s/m
α_{Tx}	10	-----	α_{Ty}	10	-----

Table 2: Select Maccs Atmos Parameters

MACCS Input	Parameter	Value
Number of Radial Angles	NUMCOR	64
Number of Radial Segments	NUMRAD	35
Weather From Files	METCOD	5 (Stratified Random Sampling)
Plume Meander Model	MNDMOD	RAF (Ramsdell and Fosmire)
Site Latitude	Latitude	39.75889
Site Longitude	Longitude	-76.26917
Samples Per Day	NSMPLS	24

Table 3: Select Maccs Early Parameters

MACCS Input	Parameter	Value
Output Control - Peak Dose	NAME	L-ICRP60ED
Exposure Duration	ENDEMP	345600 s
Cloudshine Shielding	CSFACT	1.0
Groundshine Shielding	GSHFAC	1.0
Inhalation Shielding	PROTIN	1.0
Evacuation	EVATYP	NONE
Normal Relocation Time	TIMNRM	345600 s
Normal Relocation Dose	DOSNRM	1×10^{10} Sv
Hotspot Relocation Time	TIMHOT	345600 s
Hotspot Relocation Dose	DOSHOT	1×10^{10} Sv

Electronic Supplements

Table 4: Radionuclide Class Definition and Member Elements

Radionuclide Class Name	Representative Element	Member Elements
Noble Gasses	Xe	He, Ne, Ar, Kr, Xe, Rn, H, N
Alkali Metals	Cs	Li, Na, K, Rb, Cs, Fr, Cu
Alkaline Earths	Ba	Be, Mg, Ca, Sr, Ba, Ra, Es, Fm
Halogens	I	F, Cl, Br, I, At
Chalcogens	Te	O, S, Se, Te, Po
Platinoids	Ru	Ru, Rh, Pd, Re, Os, Ir, Pt, Au, Ni
Early Transition Metals	Mo	V, Cr, Fe, Co, Mn, Nb, Mo, Tc, Ta, W
Tetravalents	Ce	Ti, Zr, Hf, Ce, Th, Pa, Np, Pu, C
Trivalents	La	Bd, Tb, Dy, Ho, Er, Tm, Yb, Lu, Am, Cm, Bk, Cf
Uranium	U	U
More Volatile Main Group	Cd	Cd, Hg, Zn, As, Sb, Pb, Tl, Bi
Less Volatile Main Group	Sn	Ga, Ge, In, Sn, Ag

Table 5: Noble Gas Specific Activity Inventories

Isotope	SOARCA Activity (Bq)	INL Heat Pipe Activity (Bq)	Ratio
Kr-85	3.789×10^{16}	1.169×10^{14}	324.131
Kr-85m	2.054×10^{18}	1.946×10^{15}	1055.672
Kr-87	2.768×10^{18}	3.816×10^{15}	725.280
Kr-88	7.022×10^{18}	5.233×10^{15}	1341.940
Xe-133	2.582×10^{18}	1.041×10^{16}	247.988
Xe-135	1.426×10^{18}	1.021×10^{16}	139.706
Xe-135m	2.054×10^{18}	1.850×10^{15}	1110.557

Table 6: Alkali Metals Specific Activity Inventories

Isotope	SOARCA Activity (Bq)	INL Heat Pipe Activity (Bq)	Ratio
Cs-134	3.605×10^{17}	1.240×10^{13}	29076.407
Cs-136	1.425×10^{17}	1.762×10^{13}	8088.602
Cs-137	3.736×10^{17}	1.044×10^{15}	357.714
Rb-86	4.378×10^{15}	1.491×10^{12}	2936.548
Rb-88	2.802×10^{18}	5.273×10^{15}	531.445

Table 7: Alkaline Earths Specific Activity Inventories

Isotope	SOARCA Activity (Bq)	INL Heat Pipe Activity (Bq)	Ratio
Ba-139	6.481×10^{18}	9.821×10^{15}	659.873
Ba-140	6.268×10^{18}	9.517×10^{15}	658.630
Sr-89	3.789×10^{18}	6.957×10^{15}	544.654
Sr-90	2.978×10^{17}	9.636×10^{14}	308.975
Sr-91	4.768×10^{18}	8.722×10^{15}	546.688
Sr-92	5.019×10^{18}	8.927×10^{15}	562.160
Ba-137m	3.545×10^{17}	9.893×10^{14}	358.358

Table 8: Halogen Specific Activity Inventories

Isotope	SOARCA Activity (Bq)	INL Heat Pipe Activity (Bq)	Ratio
I-131	3.380×10^{18}	4.643×10^{15}	728.142
I-132	4.990×10^{18}	6.974×10^{15}	715.559
I-133	7.151×10^{18}	1.036×10^{16}	690.130
I-134	8.138×10^{18}	1.207×10^{16}	674.395
I-135	6.805×10^{18}	9.865×10^{15}	689.768

Table 9: Chalcogen Specific Activity Inventories

Isotope	SOARCA Activity (Bq)	INL Heat Pipe Activity (Bq)	Ratio
Te-127	2.712×10^{17}	2.998×10^{14}	904.619
Te-127m	4.329×10^{16}	4.835×10^{13}	895.323
Te-129	8.172×10^{17}	9.503×10^{14}	859.901
Te-129m	1.554×10^{17}	1.659×10^{14}	936.531
Te-131m	6.025×10^{17}	6.248×10^{14}	964.303
Te-132	4.847×10^{18}	6.895×10^{15}	702.876
Te-131	2.894×10^{18}	4.180×10^{15}	692.320

Table 10: Platinoid Specific Activity Inventories

Isotope	SOARCA Activity (Bq)	INL Heat Pipe Activity (Bq)	Ratio
Rh-105	2.768×10^{18}	1.997×10^{15}	1385.659
Ru-103	4.828×10^{18}	5.293×10^{15}	912.206
Ru-105	3.026×10^{18}	2.069×10^{15}	1462.441
Ru-106	1.307×10^{18}	9.744×10^{14}	1341.098
Rh-103m	4.823×10^{18}	5.235×10^{15}	921.250
Rh-106	1.435×10^{18}	9.743×10^{14}	1473.231

Table 11: Early Transition Specific Activity Inventories

Isotope	SOARCA Activity (Bq)	INL Heat Pipe Activity (Bq)	Ratio
Nb-95	6.065×10^{18}	9.849×10^{15}	615.791
Co-58	0.0	0.0	0.000
Co-60	0.0	0.0	0.000
Mo-99	6.520×10^{18}	9.459×10^{15}	689.265
Tc-99m	5.835×10^{18}	8.471×10^{15}	688.803
Nb-97	6.113×10^{18}	9.244×10^{15}	661.278
Nb-97m	5.770×10^{18}	8.774×10^{15}	657.676

Table 12: Tetravalent Specific Activity Inventories

Isotope	SOARCA Activity (Bq)	INL Heat Pipe Activity (Bq)	Ratio
Ce-141	5.890×10^{18}	8.995×10^{15}	654.785
Ce-143	5.641×10^{18}	8.980×10^{15}	628.153
Ce-144	4.190×10^{18}	8.226×10^{15}	509.343
Np-239	5.613×10^{19}	7.671×10^{16}	731.653
Pu-238	6.776×10^{15}	9.367×10^{10}	72340.403
Pu-239	1.367×10^{15}	1.093×10^{13}	125.087
Pu-240	1.133×10^{15}	5.471×10^{10}	20702.431
Pu-241	3.868×10^{17}	1.074×10^{11}	3601983
Zr-95	6.108×10^{18}	9.855×10^{15}	619.856
Zr-97	6.108×10^{18}	9.228×10^{15}	659.082